Optical spectroscopy study of modifications induced in cerium dioxide by electron and ion irradiations

Jean-Marc Costantini, Gaëlle Gutierrez, Hideo Watanabe, Kazuhiro Yasuda, Seiya Takaki, Gérald Lelong, Maxime Guillaumet, William J. Weber

OPTICAL SPECTROSCOPY STUDY OF MODIFICATIONS INDUCED IN CERIUM DIOXIDE BY ELECTRON AND ION IRRADIATIONS

Jean-Marc COSTANTINI[1],

DEN-Service de Recherches Métallurgiques Appliquées, CEA, Université Paris-Saclay, F-91191, Gif-sur Yvette Cedex, France

Gaëlle GUTIERREZ,

DEN-Service de Recherches de Métallurgie Physique, CEA, Université Paris-Saclay, F-91191, Gif-sur Yvette Cedex, France

Hideo WATANABE, Kazuhiro YASUDA,

Department of Applied Quantum Physics and Nuclear Engineering, Kyushu University, 744 Motooka, Nishi-ku, Fukuoka, 819-0395 Japan

Seiya TAKAKI, Nuclear Science and Technology Directorate, Japan Atomic Energy Agency, Shirakata Shirame 2-4, Tokai 319-1195, Japan

Gérald LELONG, Maxime GUILLAUMET,

Sorbonne Université, Muséum National d'Histoire Naturelle, UMR CNRS 7590, IRD, Institut de Minéralogie, de Physique des Matériaux et de Cosmochimie, IMPMC, 75005 Paris, France

and William J. WEBER,

The University of Tennessee, Materials Science & Engineering, Knoxville, TN 37996, USA

Oak Ridge National Laboratory, Materials Science & Technology Division, Oak Ridge, TN 37831, USA

[1] Corresponding author's email : jean-marc.costantini@cea.fr

ABSTRACT

UV-visible absorption spectroscopy and Raman spectroscopy were used to study the damage production in cerium dioxide epitaxial films and sinters after irradiation by electrons for three energies (1.0, 1.4, and 2.5 MeV), and 2.4-MeV Cu ions. Neither amorphization nor specific color-center bands were detected whatsoever. Evolutions of the refractive index were derived from the interference fringes in the optical transmission spectra of epilayers after irradiation. No significant change of the refractive index occurred for the 1.0-MeV electron irradiation, whereas a maximum decrease by $28 \pm 8\%$ was deduced for the 1.4-MeV and 2.5-MeV energies. These modifications are consistent with ballistic damage in the cerium sublattice for high electron energies producing Ce^{3+} ions. However, no significant change of refractive index was found for the Cu ion irradiation. This likely stems from the high rate of Frenkel pair recombination in the collision cascades induced by more energetic recoils than for the electron irradiations, combined with electronic excitations and hole capture on Ce^{3+} ions.

PACS codes: 76.30.Kg; 78.30.-j; 78.40.-q

Keywords: Cerium dioxide; electron irradiation; heavy ion irradiation; UV-visible absorption spectroscopy; Raman spectroscopy.

I. INTRODUCTION

Fluorite-structure oxides like yttria-stabilized zirconia (ZrO_2: Y, or YSZ) and ceria (CeO_2) are known to be radiation-tolerant materials [1]. Raman spectroscopy data actually confirmed that ceria cannot be amorphized either by swift heavy ion irradiations in the electronic slowing down regime [2, 3], or lower energy ion irradiations in the nuclear-collision slowing down regime [4]. This general trend is also followed by urania (UO_2) [5], and probably by the other actinide dioxides with the same crystal structure. As a matter of fact, ceria is considered as a possible surrogate of plutonia (PuO_2), partly because Ce and Pu atoms share the same possible 3+ and 4+ oxidation states.

Actually, X-ray absorption spectroscopy [6], X-ray photoelectron spectroscopy (XPS) [7], and Raman spectroscopy [2] brought some evidence of the formation of Ce^{3+} ions, after swift heavy ion irradiations of sintered CeO_2 samples, that was associated to the appearance of a ferromagnetic state at room temperature (RT) arising from the $4f^1$ electronic configuration of these ions [8]. UV-visible absorption spectroscopy showed that a sub band-gap feature related to color centers was produced for 2.5-MeV electron irradiation of ceria single crystals, but not for the 1.0-MeV energy at similar fluences [9, 10]. On the basis of computed displacement cross sections, these point defects were assigned to ballistic damage in the Ce sublattice. Moreover, a direct experimental evidence of Ce^{3+} ions was given by electron paramagnetic resonance (EPR) spectroscopy at low temperature (< 20 K) of electron-irradiated ceria bulk single crystals for 2.5-MeV electron irradiation [10].

Although several studies using various experimental techniques were dedicated to radiation damage of ceria [6-8, 11-18], few optical spectroscopy data were reported [9, 10] to the best of our knowledge, except for Raman scattering [2-4]. This probably stems from the lack of good quality bulk single crystals or epitaxial films that are needed for optical absorption

measurements [19, 20]. Even though optical reflectivity or ellipsometry measurements on well-polished polycrystalline sintered samples are feasible, these spectra are far more difficult to process by using the Kramers-Kronig analysis [21], as was done for some oxides such as $SrTiO_3$ [22, 23] or CeO_2 [24], than the absorption data.

We report new Raman scattering and UV-visible absorption data on electron and heavy ion irradiated ceria. Those spectra yield complementary pieces of information on the radiation damage at the levels of the atomic lattice and electronic structure. The evolutions of optical transmission spectra of epilayers for electron irradiations are consistent with the cerium displacement damage in the films. The related refractive index modifications are interpreted as an indirect evidence of Ce^{3+} ion formation by elastic-collision processes. However, no such modifications are found for 2.4-MeV Cu ion irradiation. Combined point-defect recombination and electronic excitation effects in the collision cascades are thought to account for this behavior. The Raman and optical transmission spectra of epilayers and sinters show that ceria is not amorphized by electron or ion irradiations up to high fluences, even though some atomic disorder is produced in the cerium and oxygen sublattices.

II. EXPERIMENTAL PROCEDURES

High-quality epitaxial films of (100)-oriented CeO_2 (with thickness of ~1 µm) were grown by pulsed laser deposition on (100)-oriented $SrTiO_3$ (STO) substrates (with thickness of 500 µm) from MTI Corporation. The films were deposited using a 248-nm excimer laser source with an energy density of 1.5 J cm^{-2}, an oxygen partial pressure of 10 mTorr and a substrate temperature of 650°C. Ceria polycrystalline samples with thickness of 500 µm and grain sizes of ~10 µm were prepared by a sintering process at 1800 K for 12 hours, then at 1700 K for 4 hours. The CeO_2/STO samples were irradiated by electrons at the SIRIUS facility (École

Polytechnique, Palaiseau, France) under helium gas for beam intensities of ~15 µA on targets, with a flux of ~10^{13} cm^{-2} s^{-1}. Electron energies of 1.0-MeV, 1.4-MeV and 2.5-MeV were applied for various fluences up to 7.3x10^{18} cm^{-2}. The irradiation temperature did not exceed 47°C, even for high fluences. Irradiations of the CeO_2/STO samples and CeO_2 sinters were also carried out with 2.4-MeV ^{63}Cu ions at the Tandem accelerator of the Kyushu University (Fukuoka, Japan) for various fluences up to 3.0x10^{15} cm^{-2}. The low flux of ~10^{11} cm^{-2} s^{-1} prevented heating of the targets

The corresponding irradiation features, computed with the ESTAR code for electrons [25] and the SRIM2013 code for ions [26] are displayed in Tables I-II, respectively. The ion species (^{63}Cu) and energy (0.38 MeV u^{-1}) were selected so that the mean projected range in CeO_2 is about the film thickness. The mean number of displaced atoms by nuclear collisions per incident ion in the film and substrate was computed by using the following threshold displacement energies: E_d(Ce) = 45 eV, E_d(O) = 35 eV in CeO_2 [27], E_d(Sr) = 70 eV, E_d(Ti) = 140 eV, and E_d(O) = 50 eV in $SrTiO_3$ [28] (Table II). Separate simulations of collision cascades were carried out with the SRIM2013 computer code for a 1-µm thick CeO_2 film on 1-µm thick STO substrate, and a 1-µm thick CeO_2 film alone for at least 20,000 incident ions. A total number of ~6260 atoms were displaced per ion in the film, whereas a much smaller number (~490) was computed for the substrate after slowing down of Cu ions across the film thickness, by subtracting the corresponding number for the film. The Cu ions were implanted at the film/substrate interface with a range straggling of ΔR_p = 0.34 µm extending into the substrate. However, the low damage level in the substrate derives from the larger E_d values in STO. Depth profiles of the electronic stopping power (S_e) and nuclear stopping power (S_n) are displayed for CeO_2 (Fig. 1a, inset).

The electrons were transmitted through all CeO_2/STO samples with only a small difference (~10%) in total inelastic stopping power for the three different energies (Table I). The electron energy loss across the films (~1 keV) is negligible. Therefore, differences between electron irradiations are mainly due to the displacement cross sections (σ_d) for cerium and oxygen that were computed for the different electron energies with the SMOTT/POLY code [9, 29].

UV-visible transmission spectra were carried out at RT on CeO_2/STO samples with a double beam Perkin-Elmer Lambda-1050® spectrometer in the spectral range between 180 nm to 800 nm (for wave numbers from ~12,500 to 55,550 cm^{-1}) with a wavelength (λ) step and spectral resolution of 1 nm. The films were facing the light beam at normal incidence. A helium-cryostat was inserted into the sample chamber of the spectrometer to carry out low-temperature measurements from RT down to 10 K.

Micro-Raman spectra were recorded at RT in the wave-number range between 100 cm^{-1} and 1200 cm^{-1} for the virgin STO and Cu ion irradiated CeO_2/STO and CeO_2 sintered samples in a backscattering geometry using an Invia Reflex® Renishaw spectrometer coupled with an Olympus microscope containing an *x-y-z* stage. The (non-polarized) 532-nm line (i.e. photon energy ~2.33 eV) of a frequency-doubled Nd-YAG laser was focused on a 1 x 1 μm^2 spot and collected through a 100 $\times$ objective in full confocal mode. The laser power was kept below 1 mW to avoid in-beam sample annealing. Several spectra were recorded at different points of samples to check the reproducibility of measurements. The spectrometer was calibrated against a silicon wafer reference sample by using the sharp TO-LO peak at 520 $\pm$ 1 cm^{-1}.

III. RESULTS AND DATA ANALYSIS

III. 1. RAMAN SPECTROSCOPY

The Raman spectra of virgin and Cu ion-irradiated CeO_2/STO samples exhibit a strong and broad background arising from the STO substrate (Fig. 1a). Actually, for the cubic perovskite structure at RT, all the center-of-zone phonon modes are anti-symmetric (of u-type) and infra-red active only: no centro-symmetric Raman-active mode (of g-type) exists at the Γ point for q = 0, to meet the Raman selection rules for inelastic scattering [30]. Therefore, Raman scattering of a bulk STO single crystal only shows seven broad second-order (two-phonon) peaks at ~245, 305, 360, 625, 680, 725, and 1025 cm^{-1} (tagged with stars in Fig. 1a) in agreement with the literature data at 305 K [30]. This has nothing to do with the low crystalline quality of the substrate. The first-order (one-phonon) Raman spectrum was found to appear for thin films about 100 nm in thickness when the crystal symmetry was lowered due to the stress induced by lattice mismatch with the substrate [31].

The sharp and narrow center-of-zone T_{2g} peak at 461 $\pm$ 1 cm^{-1} of both virgin and irradiated ceria films with the fluorite-like structure is superimposed on top of this huge background. It is down-shifted with respect to the reference value at 467 cm^{-1} found for micro-Raman measurements in a single grain of sintered CeO_2 ceramic samples (Fig. 1b), in agreement with previous results [3]. This arises from strain accumulation in the epitaxial films upon growth due to the large lattice parameter misfit ($\Delta a_0/a_0$ ~27%).

The ratio of the T_{2g} peak intensity to that of the nearest STO background peak at ~360 cm^{-1} is increasing from ~1 for the virgin sample by ~15% for $1.0x10^{14}$ cm^{-2} (Fig. 1a). This is the signature of weak radiation damage in the substrate. Besides, three extra bands at ~185, 535, and 790 cm^{-1} appear for this fluence (tagged with arrows in in Fig. 1a). However, those bands vanish for higher fluences, and the T_{2g} peak is narrowing and slightly up-shifting by ~2 cm^{-1} for

$3.0x10^{15}$ cm^{-2}, thereby indicating a partial stress relaxation. The ratio of T_{2g} peak intensity to that of the STO peak at ~360 cm^{-1} gradually decreases from ~1.15 for $1.0x10^{14}$ cm^{-2} to ~1.05 for $3.0x10^{15}$ cm^{-2}. This means that some recovery has taken place in the substrate upon further irradiation. It is to be noted that the probed depth with 2.33-eV photons is large due the wide band gaps of ceria and STO, as discussed in the next section. As a result, it is challenging to sort out the contributions of film and substrate in these Raman spectra.

For the sintered samples, the T_{2g} peak is decreasing in intensity with fluence (for the same recording time and laser beam power) by a factor of ~30 % according to an exponential decay to a saturation (Fig. 1b, inset):

$$I = I_0 - (I_0 - I_\infty)(1 - e^{-\sigma\phi}) \quad (1)$$

where I_0 and I_∞ are the initial and saturation intensities, respectively, $\sigma = 5.4x10^{-15}$ cm^2 is the damage cross section, and ϕ is the ion fluence. Moreover, the five small and sharp satellite peaks at ~490, 512, 524, 536, and 554 cm^{-1} assigned to oxygen deficiency, and the other broad two-phonon peaks at ~230, 667, 910, 964, and 974 cm^{-1} (tagged with stars in Fig. 1b) are also clearly reduced with increasing fluence, in agreement with previous results for swift heavy ion irradiations [3]. Those side peaks vanish almost completely for $3.0x10^{15}$ cm^{-2}. However, a new band at ~585 cm^{-1} is growing with fluence (tagged with a solid arrow in Fig. 1b).

III. 2. OPTICAL ABSORPTION SPECTROSCOPY

UV-visible transmission spectra of CeO_2/STO samples at RT show clear interference patterns with nearly equi-spaced fringes as a function of wavenumber (ν) (Figs. 2-4a). The fundamental absorption edge of the as-grown film at ~26,180 cm^{-1} (for T = 0% transmittance), i.e. photon energy of 3.24 eV, is consistent with measurements on bulk single crystals giving E_g ~3.2 eV [9, 10]. The STO substrates with a wider band-gap energy: E_g = 3.25 eV, for direct transitions, and E_g = 3.75 eV, for indirect ones [32], do not contribute significantly to these spectra. No significant change in band-gap energy is recorded for the sample irradiated with 2.4-MeV Cu ions (at $3x10^{15}$ cm^{-2}) with an absorption edge at ~26,310 cm^{-1}, i.e. E_g ~3.26 eV (Fig. 4b). The absorption edge is slightly increased at low temperatures to ~26,800 cm^{-1}, i.e. E_g ~3.32 eV. However, the sub band-gap absorption feature recorded for the 1.4-MeV and 2.5-MeV electron-irradiated CeO_2 single crystals [9, 10] is not found here, due to the low absorbance (A) of this band. Accordingly, no change in color of the films was actually observed after irradiation in contrast to the bulk single crystals turning from light blue to deep green [9].

Since A = 1.2 at λ = 450 nm (ν = 22,222 cm^{-1}) for the bulk single crystal with a thickness t ~1 mm after 2.5-MeV electron irradiation [9] for a similar fluence, an absorption coefficient of α ~28 cm^{-1} is deduced from α = 2.3xA/t, giving an absorbance A ~10^{-3} for the 1-µm thick films. Such a low value precludes any detection of this band close to the absorption edge. For the laser excitation at λ = 532 nm (ν = 18,797 cm^{-1}), the mean transmittance of films (marked by a dashed line in Fig. 4a) is T ~65% and the mean absorbance is A = – log T ~19%. As a result, the mean absorption coefficient is α ~$4.3x10^3$ cm^{-1} for a thickness t = 1 µm and the probed depth in CeO_2 by Raman spectra is d ~ 1/α ~2.3 µm (for 63% attenuation of the scattered laser light). This means that the laser will probe deeper than the ceria film thickness. The probed

depth does not change significantly with fluence, unlike for amorphizable materials for which band-gap shrinkage occurs [33].

The thickness of a film on a transparent substrate can be calculated from interference fringes by the formula derived from [34, 35, 36]:

$$t = \frac{1}{2(\nu_2 n_2 - \nu_1 n_1)} \qquad (2)$$

where ν_1 and ν_2 are the wavenumbers of two adjacent transmission spectrum maxima (or minima) with the corresponding refractive indices n_1 and n_2, respectively. The refractive index of the transparent STO substrate (n_s = 2.43 at λ = 550 nm, ν = 18,182cm^{-1} and n_s = 2.54 at λ = 450 nm, ν = 22,222 cm^{-1}) [37] does not contribute to Eq. (2), which is deduced from the basic condition for interferences in the films [34]. A validation of refractive index determination with Eq. (2) was carried out for reference yttrium iron garnet (YIG) epitaxial films of known thicknesses measured by interferometry [33].

As a first approximation, we assumed that $n_1 \sim n_2 \sim n_0$ = 2.3 for ceria (value for λ = 550 nm, ν = 18,182 cm^{-1} at RT), which is the mean value in this wavenumber range: an increase of 0.1 from this value was found for λ = 450 nm (ν = 22,222 cm^{-1}) regardless of temperature [19]. Using the three fringes for the virgin sample far from the absorption edge (Fig. 2), we get thicknesses of 650 nm and 570 nm with a mean value of t = 610 $\pm$ 40 nm from Eq. (2), which is consistent with the expected value of ~1 µm for the as-grown films. The first maximum close to the absorption edge was discarded. Scattered values are generally obtained by this method when different fringe doublets are used [34].

For the 1.4-MeV and 2.5-MeV electron irradiated films, the fringe spacing of $\Delta\nu = (\nu_2 - \nu_1)$ is increasing with fluence as compared to the virgin sample (Figs. 2-3). In contrast, no significant changes in $\Delta\nu$ are found for the 1.0-MeV energy, even though the fringe system is shifted with respect to the virgin film (Fig. 3). A similar behavior is observed for the Cu ion irradiation with almost no variation of the $\Delta\nu$ values even for the highest fluence (Fig. 4a). Besides, no significant changes in fringe spacing are observed at low temperatures, even though the absorption edge is shifted to a higher wave number (Fig. 4b). Now using the mean thickness of 610 nm, approximate values of the refractive index (n) were deduced for irradiated CeO_2/STO samples by using the wavenumber maxima (ν_1 and ν_2) in Eq. (2) and assuming that $n \sim n_1 \sim n_2$. The values of $n = (2t\Delta\nu)^{-1}$ are plotted versus fluence for the different fringe doublets with a maximum experimental error ($\pm$ 10%) including the error on thickness and fringe wavenumber determination (Figs. 2 and 4a, insets). Fringes close to the absorption edge were not used because they generally yield unreliable results [34].

Since the fringe system is shifted after irradiation, the refractive index cannot be measured for exactly the same wavenumber as in the virgin sample. As a result, only the evolution of the mean n-value for $\nu \sim$18,000 cm^{-1} was deduced from these spectra by using Eq. (2) for t = 610 nm (Fig. 2 and 4a, insets). A fit of the 2.5-MeV electron data with a similar function as Eq. (1) yields a damage cross section of $\sigma = 6.0 \times 10^{-18}$ cm^2 for $n_\infty = 1.8$ (Fig. 2, inset). No significant variations are deduced for the 1.0-MeV electron and Cu-ion data with average values of 2.46 and 2.35 respectively (Fig. 2 and 4a, insets).

Another classical analysis, known as the envelope method, was often applied by using the maximum (T_M) and minimum (T_m) transmittance values interpolated for various wavelengths on the spectra [34, 35], such as for ceria films on yttria-stabilized zirconia (YSZ)

or MgO substrates [20]. For the region of weak and medium optical absorption at normal incidence, it was shown that:

$$n = [N + (N^2 + n_s^2)^{1/2}]^{1/2} \quad (3)$$

where:

$$N = 2n_s \frac{\Delta T}{T_m T_M} + \frac{n_s^2+1}{2} \quad (4)$$

The film refractive index (n) can be deduced from the T_M and T_m values knowing the substrate refractive index (n_s) for any wavenumber. Such a method was used to process the modulated transmission spectra with non equispaced fringes recorded as a function of wavelength for various thin films [20, 34, 35]. However, the interpolation with polynomial functions [35] is rendered difficult in the present case due to the very small $\Delta T = (T_M - T_m)$ ~2% differences, as compared to the literature data showing ΔT values ranging between ~30% and 50% in the same wavenumber range [34, 35]. This stems from the larger refractive index contrast in the latter cases of amorphous Si (n ~3.4) [34] or amorphous As_2S_3 (n ~2.4) [35] films on a glass substrate (n_s ~1.6) in the visible range. The roughness of film surfaces also induces a decrease of ΔT and flattening of fringes [34]: ΔT values of ~10% were actually found for porous ceria films on YSZ [20]. The increase of ΔT to 5% for the Cu irradiation at the highest fluence (Fig. 4a) might arise from an increase of the $(n - n_s)$ difference. However, significant estimations cannot be obtained by using this approach in the present case of weak oscillations for such low ΔT values.

Moreover, such analysis requires the knowledge of the dependence of n_s on fluence at the film/substrate interface. Variations of the refractive index for a perovskite oxide such as

$LiNbO_3$ were actually reported after ion implantations [38-40]. However, the n-values deduced from Eq. (2) are independent of evolutions of n_s upon irradiation, in contrast to the envelope method. The normal-incidence reflectance value deduced from Fresnel's equation at the ceria film surface is R ~15% for n = 2.3, whereas the reflectance at the film/substrate interface is very low (R ~$7.5x10^{-4}$) for n_s = 2.43 at λ = 500 nm (ν = 18,182 cm^{-1}), for the virgin sample. This can account for the weak oscillations of fringes in the ceria films as opposed to the above-mentioned cases. The dispersion in the T_M and T_m values for different samples may be assigned to scattering of the CeO_2/STO sample thickness ($\pm$ 5%) and variations in reflectance at the sample surface varying from R ~15% to 21% in dependence to the film refractive index.

In agreement with this qualitative analysis of spectra, n is decreasing with fluence to a maximum relative variation of $\Delta n/n_0 \sim -28 \pm 8\%$ for 2.5-MeV electrons at $3x10^{17}$ cm^{-2} and for 1.4-MeV electrons at $4.2x10^{18}$ cm^{-2}, whereas no significant variations with a huge scattering are derived for the 1.0-MeV energy spectra in the same range of fluences (Fig. 1a, inset), as well as for the Cu-ion irradiation, even though the oscillations are enhanced for $3.0x10^{15}$ cm^{-2} (Fig. 4a, inset).

IV. DISCUSSION

IV. 1 Raman spectroscopy data

Raman spectra show that no striking changes of the sharp T_{2g} peak of CeO_2 films occur for the Cu ion irradiation up to a fluence of $3.0x10^{15}$ cm^{-2} (Fig. 1a), corresponding to a dose of ~7.5 displacement per atom (dpa), using the mean number of displaced atoms per path length unit of ~$6.3x10^3$ μm^{-1} (Table II) and atomic density of N_a = $2.52x10^{22}$ cm^{-3} (for a lattice parameter of $CeO_{2.0}$, a = 0.541 nm). In contrast for sintered samples, a limited decrease in intensity of the T_{2g} peak by 30% (Fig. 1b, inset), but clear reduction of the sharp satellite peaks

and broad two-phonon bands occur for the same fluences, as observed previously for high electronic stopping powers [3].

However, in the present case, we assume that the damage derives primarily from the nuclear stopping power, for such a low electronic stopping power (Table II) [3], even though $S_e > S_n$ on the major part of the film thickness (Fig. 1a, inset). This is in agreement with a recent study for 2.0-MeV Au ion irradiation up to 1.3×10^{16} cm^{-2} (corresponding to 100 dpa) [4]. These results confirm that the fluorite structure of ceria is quite a radiation-resistant structure up very large doses. Owing to the low projected range (R_p = 170 nm) of the 2.0-MeV Au ions in ceria, the light scattered by the film contained both contributions of the damaged and pristine ceria [4]. Instead, in the present study, the whole damaged film thickness was probed, as discussed in the previous section.

Anyway, as explained above, a significant part of the Raman scattering signal is arising from the STO substrate in all these measurements, owing to the high transmittance (T ~65%) of the films (Fig. 4a) for the various laser wavelengths (λ = 473, 532, and 785 nm, i.e. ν = 21,142, 18,797, and 12,739 cm^{-1}) used in the present study and by Graham et al. [4]. As a result, the broad second-order scattering from the substrate (Fig. 1a) should be subtracted from spectra to obtain the T_{2g} peak evolution with irradiation [4], unlike for self-supported sintered samples (Fig. 1b) [3].

However, the new broad bands appearing at ~185, 535, and 790 cm^{-1} for CeO_2/STO sample at the fluence of 1×10^{14} cm^{-2} (Fig. 1a) are likely associated to defects induced by irradiation. Similar extra bands called D_1 and D_2 centered at ~550 and 590 cm^{-1} were also reported for the 2.0-MeV Au ion irradiation and mainly assigned to the substrate contribution [4]. For the self-supported sintered samples, a new broad band at ~585 cm^{-1} is growing with fluence (Fig. 1b). Such a band was already recorded after swift heavy ion irradiations for similar

high fluences and attributed to oxygen vacancies [2, 3]. This means that the whole damaged films do contribute to these extra bands.

Hence, the extra bands at ~535 and 585 cm^{-1} likely derive from displacive damage in the oxygen sublattice of ceria induced by Cu ions. These defect bands vanish for high fluences due to in-beam dynamic annealing. The decay of satellite peaks and two-phonon bands for sintered samples is probably stemming from the gradual disordering of the oxygen sublattice, yet without reaching amorphization, since the T_{2g} peak does not strongly decreases in intensity (Fig. 1b, inset). A decrease by ~30% is observed to compare with ~50% for swift heavy ion irradiations [3].The related damage cross section ($\sigma = 5.4x10^{-15}$ cm^2) is clearly lower than the value ($\sigma = 2.0x10^{-13}cm^2$) previously obtained for 36-MeV W ions in the electronic stopping power regime [3]. The latter value was reproduced by the inelastic thermal spike model of ion track formation [3], whereas the former value corresponds to an atomic collision cascade overlap process. In contrast, besides the sharp T_{2g} peak, the Raman spectrum of a CeO_2 single crystal featured two weak and broad bands centered at ~605 and 672 cm^{-1} related to the original oxygen deficiency, that did not show any modifications after 2.5-MeV electron irradiation up to $7.3x10^{18}$ cm^{-2} [10].

IV.2 Optical transmission data

As such, the UV-visible transmission data of ion-irradiated films are consistent with Raman spectra, since no clear red-shift of the fundamental absorption edge due to amorphization is found. Actually, neither absorption bands arising from color-center formation in the films or substrate, nor increase of Urbach tail are recorded after electron or ion irradiations, unlike for amorphizable oxides such as YIG [33]. As a matter of fact, no amorphization or crystalline phase changes of ceria was ever achieved by electron or heavy

ion irradiations, even for high fluences [1, 3, 4, 6, 7]. Therefore, we assigned the observed changes in interference fringes to modifications of the film refractive index, and not to changes in thickness related to mass density modifications. The band-gap energy decreases by ~0.04 eV from 300 K to 10 K (Fig. 4b), as is generally found for semiconductors [21], e.g. ~0.1 eV for germanium between 300 K and 77 K [39]. Yet, no significant changes in $\Delta\nu$ and refractive index occur in this temperature range despite the shift of interference fringes arising from the blue-shift of absorption edge.

The decrease of refractive index for the 1.4-MeV and 2.5-MeV electrons is consistent with radiation damage in the cerium sublattice in agreement with the optical absorption data of single crystals [9, 10]. Actually, oxygen atoms should be displaced by 1.0-MeV electrons for E_d = 35 eV, whereas cerium should be displaced for electron energies higher than 1.3 MeV by taking E_d = 45 eV [9]. This set of E_d values was recommended for CeO_2 [27]. Once again, the very small difference in inelastic stopping power for these three electron energies (Table I) cannot account for the observed effects on the refractive index. The damage cross section (σ = 6.0x10^{-18} cm^2) is typical of an elastic-collision process involving point-defect recombination, as found for F-center formation in YSZ by electron irradiation [42]. The saturation value is proportional to σ_d/σ, with a cross section $\sigma = \sigma_r + 2\sigma_d V_r$, where σ_r and V_r are the recombination cross section and the recombination volume in number of lattice sites, respectively [42].

These data can be rescaled by the number of displacement per Ce atom (dpa), such as dpa = $\sigma_d \phi$, where σ_d is the displacement cross section of Ce atoms [9] and ϕ is the electron fluence. For 2.5-MeV electrons, σ_d = 56.7 b [9], giving 1.7x10^{-5} dpa for ϕ = 3x10^{17} cm^{-2}. Hence, the concentration of displaced Ce atoms is of $N_d = N_a$ dpa ~4.3x10^{17} cm^{-3} and the total number of displaced Ce atoms is of ~4.3x10^{13}, for a film with surface of ~1 cm² and t ~1 μm. For 1.4-MeV electrons, one has σ_d = 4.1 b [9] that gives 1.7x10^{-5} dpa for ϕ = 4.2x10^{18} cm^{-2}. The plot of

the refractive index as a function of dpa shows a clear decrease for ~$2x10^{-5}$ dpa within experimental errors, regardless of electron energy and fluence (Fig. 5).

Actually, these estimates are consistent with the EPR data of a CeO_2 single crystal irradiated with 2.5-MeV electrons at $\phi = 1.5x10^{18}$ cm^{-2} [10]. The EPR spectrum at 4.5 K gave a total number of Ce^{3+} ions of ~10^{14} for a sample volume of ~$5x10^{-4}$ cm^3 corresponding to a concentration of ~$2x10^{17}$ cm^{-3}. It is to be noted that σ_d values for oxygen atoms do not vary significantly from 1.0 MeV to 2.5 MeV [9]. As such, the variations of refractive index cannot be accounted for by the displacement damage in the oxygen sublattice.

The impact of such point-defect production on the refractive index is not straightforward. As a matter of fact, few older studies were dedicated to the modifications of refractive index by ion irradiations for optoelectronics applications, which is a complex issue depending on the defect species and concentration. The ordinary refractive index in α-SiO_2 quartz ($n_0 = 1.54$) for $\lambda = 575$ nm was reduced ($\Delta n/n_0 = -4.2\%$) by heavy ion implantations in the 100-keV range at the saturation of damage, corresponding to full amorphization [40], whereas an increase was found ($\Delta n/n_0 \sim +1\%$) for (amorphous) fused silica ($n_0 = 1.46$) under the same conditions [39].

For $LiNbO_3$ ($n_0 = 2.27$), optical wave guides were prepared by helium ion implantation for an energy of ~2.0-MeV with a refractive index decrease versus depth [39, 40]. Heavy-ion implantations also induced a decrease of the ordinary refractive index for $\lambda = 632.8$ nm: $\Delta n = -0.165 \pm 0.015$ at the saturation of damage for 150-keV N ions [39], and $\Delta n/n_0 \sim -$ 10%-15% for 60-keV Ar ions [38]. As discussed above, the possible effect on n_s has no impact on the evaluation of refractive index of the films.

A recent study attempted to tailor the refractive index of nano-diamonds ($n_0 = 2.41$, for $\lambda = 632.8$ nm) in introducing NV^- centers (nitrogen-carbon vacancy complexes) by 2-MeV

or 3-MeV proton implantation [43]. The refractive index increased linearly as a function of the carbon vacancy concentration up to a maximum value for $\Delta n/n_0 \sim +4\%$, in agreement with the typical increase of $\Delta n = +0.1$ for 20-keV C ion implantation [44].

The modifications of SiO_2 were attributed to the effect of volume change on the refractive index on the basis of the Lorentz-Lorenz (or Clausius-Mossotti) equation, for insulators [39], like for $LiNbO_3$ [38, 40]. A derivation of this equation yields [40]:

$$\frac{\Delta n}{n_0} = \frac{(n_0^2-1)(n_0^2+2)}{6n_0^2}\left(-\frac{\Delta V}{V} + \frac{\Delta \alpha}{\alpha} + F\right) \qquad (5)$$

where α is the electronic polarizability of bonds, V is the molecular volume, and F is a structural factor of the irradiated material. The volume effect is generally dominating, but changes can be positive or negative in sign depending on the respective contributions of dilation and polarizability. In the case of covalent solids like diamond, stronger effects of the polarizability are expected [43], rather than in ionic solids like lithium niobate [38, 40]. The temperature dependence can also be derived from Eq. (5) by assuming no changes in polarizability and structural factor. For a temperature decrease from 300 K to 10 K, one gets a contraction of $\Delta V/V \sim -0.2\%$ and $\Delta n/n_0 \sim +0.2\%$ for $n_0 = 2.3$, by using a mean thermal expansion coefficient of $\beta = 7 \times 10^{-6}$ K^{-1} for ceria in this temperature range [45]. Such a very small variation of $\Delta n \sim 4.7 \times 10^{-3}$ can only be detected by interferometric techniques, but not by the present optical transmission spectra (Fig. 4b).

We surmise that the observed decrease in ceria could stem from the formation of highly charged Ce vacancies producing a local volume expansion due to Coulomb repulsive forces in the ionic lattice. In the case of α-quartz ($n_0 = 1.54$), Eq. (5) yields $\Delta n/n_0 \sim -8\%$ for a

volume expansion of $\Delta V/V = 19\%$ [39]. As such, it overestimates the observed refractive index variation by a factor around two. The other positive terms in Eq. (5) might counterbalance the negative volume effect. On the other hand, the effect on the electronic polarizability ($\Delta\alpha/\alpha$) in α-quartz was estimated to $\Delta n = + 0.01$ from Eq. (5) at the saturation of damage with 150-keV Ar ion implantation [39]. In the present case, Eq. (5) would yield a much larger value of $\Delta V/V \sim 29\%$ for $\Delta n/n_0 \sim -28\%$ and $n_0 = 2.3$. Therefore, such a large refractive-index decrease cannot be solely related to vacancies, but also to the contribution of Ce^{3+} interstitials.

However, no direct evidence of paramagnetic cerium vacancies (V_{Ce}''') was found from EPR spectra [10]. Only a clear signal was assigned to Ce^{3+} ions for 2.5-MeV electrons, but not for the 1.0-MeV energy. A weak EPR signal was recorded for the 1.4-MeV electron irradiation. This was attributed to a reduction process induced by the displacement damage [10]. Regarding the Cu ion irradiation, no such modifications of refractive index are found even though a higher number of displaced atoms is produced (Table II) with respect to electrons. Actually, previous studies using swift heavy ion irradiations did not find any evidence of Ce^{3+} ion formation on the basis of Electron Energy Loss Spectroscopy measurements [16], whereas XPS measurements found an increase of the Ce^{3+} concentration after 2.0-MeV He ion irradiation [13].

It is likely that recombination of Frenkel pairs is enhanced in the dense collision cascades induced by more energetic Ce and O recoiling atoms (with kinetic energies $\leq$ 2.0 MeV) for Cu ions than for electron irradiations producing a more dilute damage and small displacement cascades induced by low-energy recoils [10]. Moreover, the much larger inelastic stopping power than for electrons (Tables I-II) may also contribute to the disappearance of Ce^{3+} ions. Indeed, the number of electron-hole pairs (N_{e-h}) produced per

Cu ion outweighs the number per electron by a factor of 1900: i.e. $N_{e-h} \sim \frac{\delta E}{3E_g} \sim 10^5$ pairs per ion [46], for an energy loss of δE = 1900 keV across the film thickness. It is liable to assume that free-hole capture on Ce^{3+} ions may restore the Ce^{4+} lattice ions. Grain growth in nanocrystalline CeO_2 was found after 1.0-MeV Si ion irradiation for smaller values of electronic and nuclear stopping powers [47]. It is the combination of these two kinds of processes that led to grain growth.

In summary, we conclude that the 1.4-MeV and 2.5-MeV electron irradiations have generated a preferential damage in the cerium sublattice by elastic collisions that could account for the modifications of optical properties of ceria films. It is also concluded that the Ce^{3+} ions induced by such a process should contribute to the clear decrease of the ceria film refractive index. No amorphization of ceria films and sinters was achieved after electron of ion irradiations whatsoever, thereby confirming the great radiation resistance of this material.

V. CONCLUSIONS

Epitaxial films of cerium dioxide were irradiated by electrons for energies of 1.0, 1.4, and 2.5 MeV, while both epilayers and sintered samples were irradiated by 2.4-MeV Cu ions up to high fluences. Raman scattering and UV-visible transmission spectra show that amorphization is not produced by these irradiations. However, new defect bands appear in Raman spectra for both kinds of samples. The UV-visible transmission spectra of epitaxial films exhibit clear changes of the interference fringe spacing after 1.4-MeV and 2.5-MeV electron irradiations, but not for the 1.0-MeV energy. The large refractive index decrease by $\sim 28 \pm 8\%$ deduced from these spectra is assigned to Ce^{3+} interstitials induced by elastic collisions. Spectroscopic ellipsometry measurements may be used to cross-check these results. In contrast, no such modifications are found for the Cu ion irradiation. This might originate from

atomic and electronic recombination processes in the dense collision cascades, as opposed to the dilute point defect production and low inelastic stopping power for electrons.

ACKNOWLEDGMENTS: We thank the French EMIR network for supporting this research program. The authors are also indebted to Bruno Boizot and Olivier Cavani (École Polytechnique, Palaiseau, France) for their help during the electron irradiations. One of the authors (W. J. W.) was supported by the U.S. Department of Energy, Office of Science, Basic Energy Sciences, Materials Science & Engineering Division. The CeO_2 thin films were grown at the Center for Nanophase Materials Sciences, which is a DOE Office of Science User Facility.

REFERENCES

[1] J.-M. Costantini, F. Beuneu, and W. J. Weber, "*Radiation Damage in Cubic-Stabilized Zirconia and Ceria*", in "*Properties of Fluorite Structure Materials*", Eds. P. Vajda and J. M. Costantini (Nova Science Publishers, New York, 2013), Chapter 5.

[2] K. Ohhara, N. Ishikawa, S. Sakai, Y. Matsumoto, O. Michikami, and Y. Ohta, Nucl. Instr. and Meth. B 267 (2009) 973.

[3] J.-M. Costantini, S. Miro, G. Gutierrez, K. Yasuda, S. Takaki, N. Ishikawa, and M. Toulemonde, J. Appl. Phys., 122 (2017) 205901.

[4] J. T. Graham, Y. Zhang, and W. J. Weber, J. Nucl. Mater., 498 (2018) 400.

[5] Hj. Matzke, A. Turos, and G. Linker, Nucl. Instr. and Meth., B 91 (1994) 294.

[6] H. Ohno, A. Iwase, D. Matsumura, Y. Nishihata, J. Mizuki, N. Ishikawa, Y. Baba, N. Hirao, T. Sonoda, and M. Kinoshita, Nucl. Instr. and Meth., B 266 (2008) 3013.

[7] A. Iwase, H. Ohno, N. Ishikawa, Y. Baba, N. Hirao, T. Sonoda, and M. Kinoshita, Nucl. Instr. and Meth., B 267 (2009) 969.

[8] K. Shimizu, S. Kosugi, Y. Tahara, K. Yasunaga, Y. Kaneta, N. Ishikawa, and F. Hori, Nucl. Instr. and Meth. B 286 (2012) 291.

[9] J.-M. Costantini, G. Lelong, M. Guillaumet, W. J. Weber, S. Takaki, and K. Yasuda, J. Phys.: Condens. Matter, 28 (2016) 325901.

[10] J.-M. Costantini, L. Binet, N. Touati, G. Lelong, M. Guillaumet, and W. J. Weber, J. Appl. Phys., 123 (2018) 025901.

[11] N. Ishikawa, Y. Chimi, O. Michikami, Y. Ohta, K. Ohhara, M. Lang, and R. Neumann, Nucl. Instr. and Meth., B 266 (2008) 3033.

[12] N. Ishikawa, and K. Takegahara, Nucl. Instr. and Meth., B 272 (2012) 227.

[13] A. Kumar, R. Devanathan, V. Shutthanandan, S. V. N. T. Kuchibhatla, A. S. Karakoti, Y. Yong, S. Thevuthasan, and S. Seal, J. Phys. Chem. C 116 (2012) 361.

[14] T. Kishino, K. Shimizu, Y. Saitoh, N. Ishikawa, F. Hori, and A. Iwase, Nucl. Instr. and Meth., B 314 (2013) 191.

[15] K. Yasuda, M. Etoh, K. Sawada, T. Yamamoto, K. Yasunaga, S. Matsumura, and N. Ishikawa, Nucl. Instr. and Meth., 314 (2013) 185.

[16] C. A. Yablinsky, R. Devanathan, J. Pakarinen, J. Gan, D. Severin, C. Trautmann, and T. R. Allen, J. Mater. Res. 30 (2015) 1473.

[17] S. Takaki, K. Yasuda, T. Yamamoto, S. Matsumura, and N. Ishikawa, Progress in Nucl. Energy (2016)

[18] R. I. Palomares, J. Shamblin, C. L. Tracy, J. Neuefeind, R. C. Ewing, C. Trautmann, and M. Lang, J. Mater. Chem. A 5 (2017) 12193.

[19] G. Hass, J. B. Ramsey, and R. Thun, J. Opt. Soc. Am., 48 (1958) 324.

[20] T. S. Oh, Yu. S. Tokpanov, Y. Hao, W. Jung, and S. M. Haile, J. Appl. Phys., 112 (2012) 103535.

[21] J. I. Pankove, "*Optical Processes in Semiconductors*" (Dover, New York, 1975).

[22] A. S. Barker, and M. Tinkham, Phys. Rev. 125 (1962) 1527.

[23] K. Kamaras, K. L. Barth, F. Keilmann, R. Henn, M. Reedyk, C. Thomsen, M. Cardona, J. K. Kircher, P. L. Richards, and J. L. Stehlé, J. Appl. Phys., 78 (1995) 1235.

[24] S. Guo, H. Atwin, S. N. Jacobsen, K. Jearendahl, and U. Helmersson, J. Appl. Phys. 77 (1995) 5369.

[25] "*Stopping Powers for Electrons and Positrons*", International Commission on Radiation Units and Measurements, ICRU Report 37 (1984). (http://physics.nist.gov/PhysRefData/contents-radi.html).

[26] J. P. Biersack, and L. G. Haggmark, Nucl. Instr. and Meth., 174 (1980) 257. (www.srim.org)

[27] S. J. Zinkle, and C. Kinoshita, J. Nucl. Mater., 251 (1997) 200.

[28] B. S. Thomas, N. A. Marks, and B. D. Begg, Nucl. Instr. and Meth., 254 (2007) 211.

[29] J. M. Costantini, and F. Beuneu, Phys. Stat. Sol. (c), 4 (2007) 1258.

[30] C. H. Perry, J. H. Fertel, and T. F. McNeilly, J. Chem. Phys. 47 (1967) 1619.

[31] A. A. Sirenko, I. A. Akimov, J. R. Fox, A. M. Clark, H. C. Li, W. Si, and X. X. Xi, Phys. Rev. Lett. 82 (1999) 4500.

[32] K. van Benthem, C. Elsässer, and R. H. French, J. Appl. Phys. 90 (2001) 6156.

[33] J.-M. Costantini, S. Miro, G. Lelong, M. Guillaumet, and M.Toulemonde, Philos. Mag., 98 (2017)312.

[34] R. Swanepoel, J. Phys. E: Sci. Instrum., 16 (1983) 1214.

[35] E. Marquez, J. Ramirez-Malot, P. Villarest, R. Jiménez-Garay, P. J. S. Ewen and A. E. Owen, J. Phys. D: Appl. Phys., 25 (1992) 535.

[36] M. Caglar, Y. Caglar, and S. Ilican, J. Optoelec. and Adv. Materials, 8 (2006) 1410.

[37] M. J. Dodge. Refractive Index, in M. J. Weber (ed.), Handbook of Laser Science and Technology, Volume IV, Optical Material: Part 2, CRC Press, Boca Raton, 1986 (as cited in Handbook of Optics, 3rd edition, Vol. 4. McGraw-Hill 2009).

[38] D. T. Y. Wei, W. W. Lee, and R. L Bloom, Appl. Phys. Lett., 25 (1974) 329.

[39] G. Götz, "*Optoelectronics Materials*", in "*Ion Beam Modification of Insulators*", Eds P. Mazzoldi and G. W. Arnold (Elsevier, Amsterdam, 1987), Chapter 10.

[40] P. D. Townsend, Nucl. Instr. and Meth., B 46 (1990) 18.

[41] K. Seeger, "*Semiconductor Physics: An Introduction*" Springer Series in Solid-State Sciences vol. 40 (Springer, Berlin, 1991).

[42] J. M. Costantini, and F. Beuneu, J. Phys.: Condens. Matter, 23 (2011) 115902.

[43] S. Lagomarsino, P. Olivero, S. Calusi, D. Gatto Monticone, L. Giuntini, M. Massi, S. Sciortino, A. Sytchkova, A. Sordini, and M. Vannoni, Optics Express, 20 (2012) 19382.

[44] R. L. Hines, Phys. Rev. 138 (1965) A1747.

[45] H. Hayashi, M. Kanoh , C. J. Quan , H. Inaba , S. Wang , M. Dokiya , and H. Tagawa, Solid State Ionics 132 (2000) 227.

[46] R. C. Alig, and S. Bloom, Phys. Rev. Lett, 35 (1975) 1522.

[47] Y. Zhang, D. S. Aidhy,T. Varga, S. Moll, P. D. Edmondson, F. Namavar, K. Jin, Ch. N. Ostrouchov, and W. J. Weber, Phys. Chem. Chem. Phys. 16 (2014) 8051.

Table I: Electron irradiation features for CeO_2 (mass density = 7.215 g cm^{-3}) and $SrTiO_3$ (mass density = 5.11 g cm^{-3}) with mean ionization energies of I = 407.6 eV and I = 249 eV respectively: incident energy (E), total inelastic stopping power $(-dE/dx)_{inel}$, and CSDA range (R) computed with the ESTAR code [25].

E (MeV)	$(-dE/dx)_{inel}$ (keV μm^{-1})	R (mm)	$(-dE/dx)_{inel}$ (keV μm^{-1})	R (mm)
Material	CeO_2	CeO_2	$SrTiO_3$	$SrTiO_3$
1.0	0.90	0.9	0.70	1.2
1.4	0.92	1.5	0.70	1.9
2.5	1.0	2.5	0.74	3.3

Table II: Ion irradiation features for 2.4-MeV ^{63}Cu ions in CeO_2 (mass density = 7.215 g cm^{-3}): electronic stopping power ($S_e = (-dE/dx)_e$), nuclear stopping power ($S_n = (-dE/dx)_n$), and mean projected range (R_p) with range straggling (ΔR_p), computed with the SRIM2013 code [26].

S_e (keV μm^{-1})	S_n (keV μm^{-1})	S_e/S_n	R_p (μm)	ΔR_p (μm)
1900	470	4.0	1.0	0.34

Figure 1: Raman spectra of STO and CeO_2/STO samples (a) and self-supported sintered CeO_2 samples (b) irradiated with 2.4-MeV Cu ions (defect peaks are tagged with arrows). Insets: depth profiles of electronic stopping power (S_e, dashed curve) and nuclear stopping power (S_n, solid curve) for 2.4-MeV ^{63}Cu ions in CeO_2 (a), and intensity of the T_{2g} peak versus fluence with a least-squares fit (dashed curve) using Eq. (1) (b).

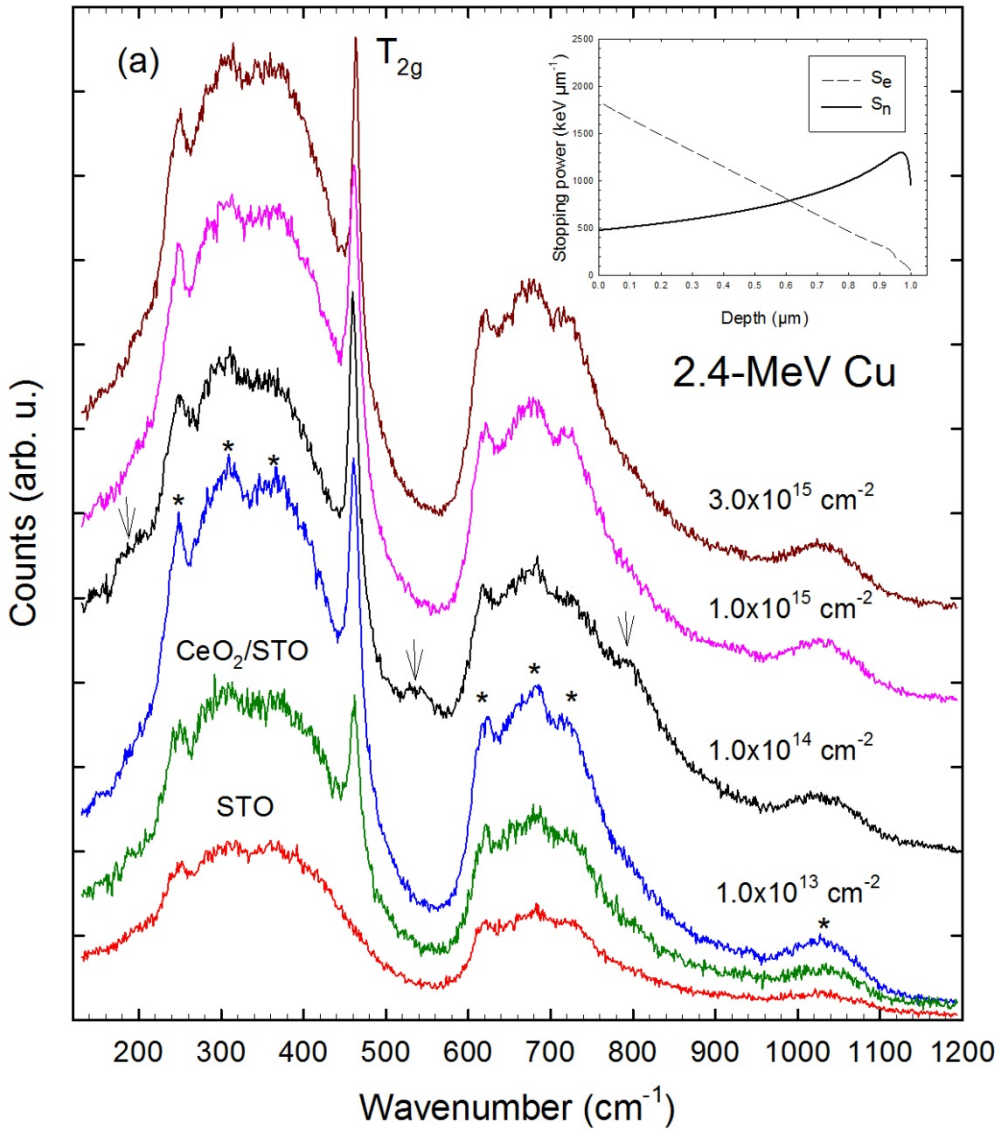

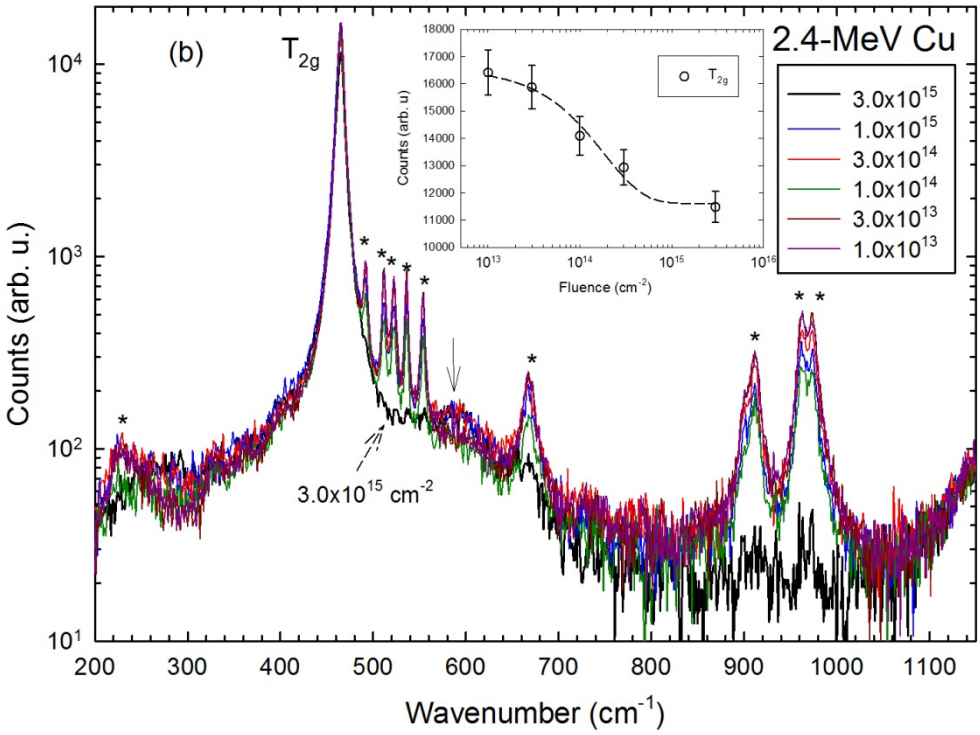
(b)
T_{2g}
2.4-MeV Cu
3.0x10^15
1.0x10^15
3.0x10^14
1.0x10^14
3.0x10^13
1.0x10^13
3.0x10^15 cm^-2
Counts (arb. u.)
Wavenumber (cm^-1)
Fluence (cm^-2)
Counts (arb. u)

Figure 2: UV-visible transmission spectra at RT of virgin (dotted curve) and electron-irradiated (solid curves) CeO_2 thin films on STO substrates for 2.5-MeV electrons at various fluences. Inset: mean refractive index versus fluence for the three electron energies and different fringe doublets. The dashed horizontal line marks the average value (n = 2.46) for 1.0-MeV and low-fluence 2.5-MeV data. The dashed curve is a trial-and-error fit using Eq. (1).

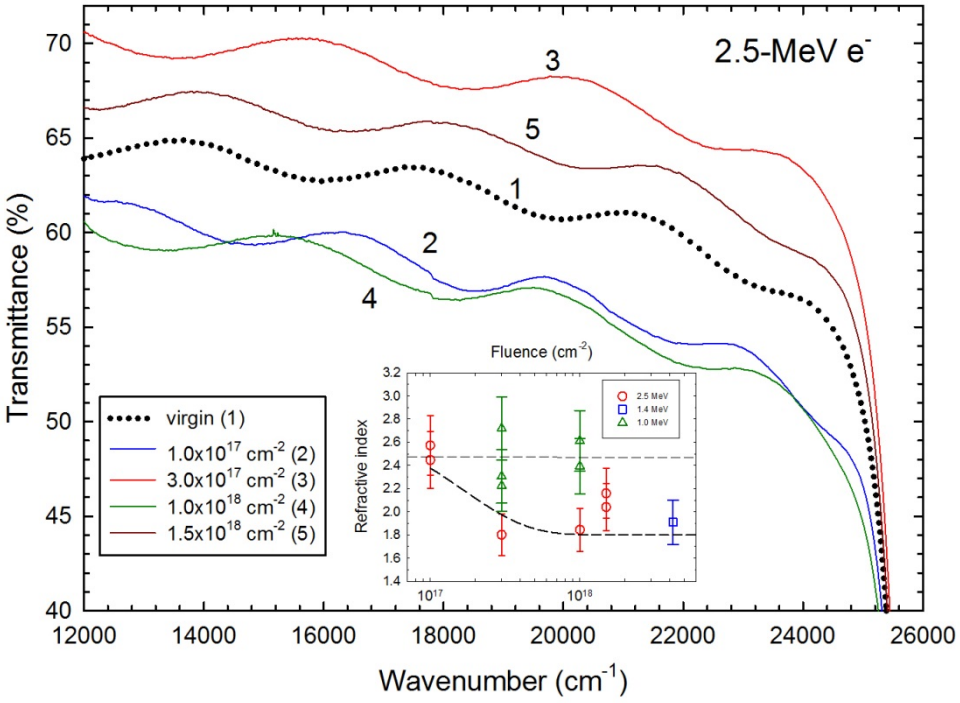

Figure 3: UV-visible transmission spectra at RT of virgin (dotted curve) and electron-irradiated CeO_2 thin films on STO substrates for 1.0-MeV (dashed curves) and 1.4-MeV (solid curves) electrons at various fluences.

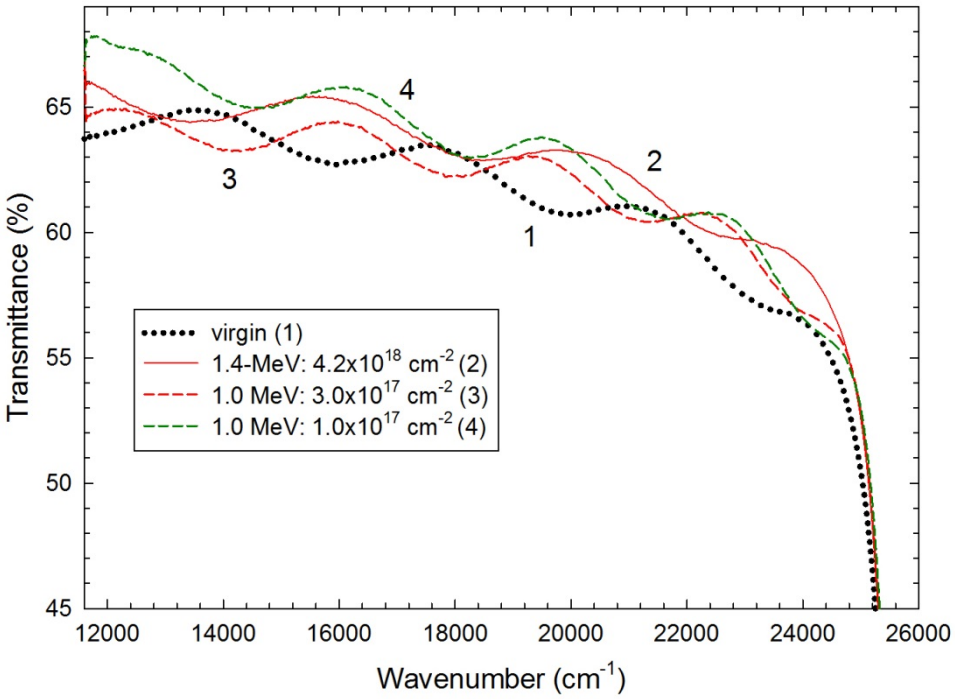

Figure 4: UV-visible transmission spectra of virgin (dotted curve) and 2.4-MeV Cu ion-irradiated (solid curves) CeO_2 thin films on STO substrates for various fluences at RT (a), and at various temperatures for the fluence of $3.0x10^{15}$ cm^{-2} (b). The dashed vertical line marks the laser wave number in Raman experiments. Inset: mean refractive index versus fluence for different fringe doublets. The dashed horizontal line marks the average value (n = 2.35).

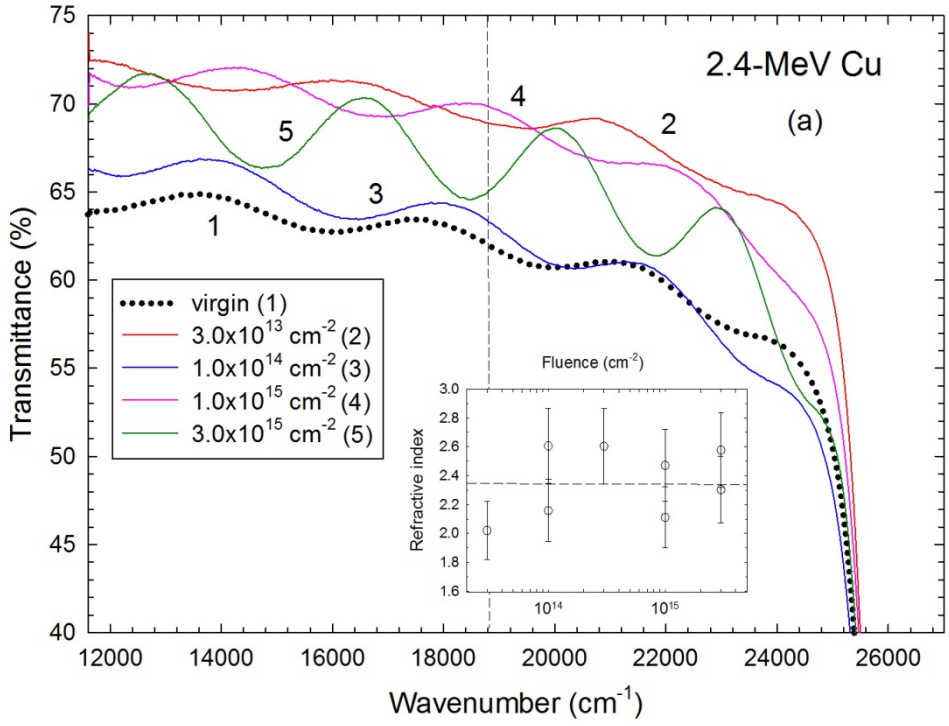

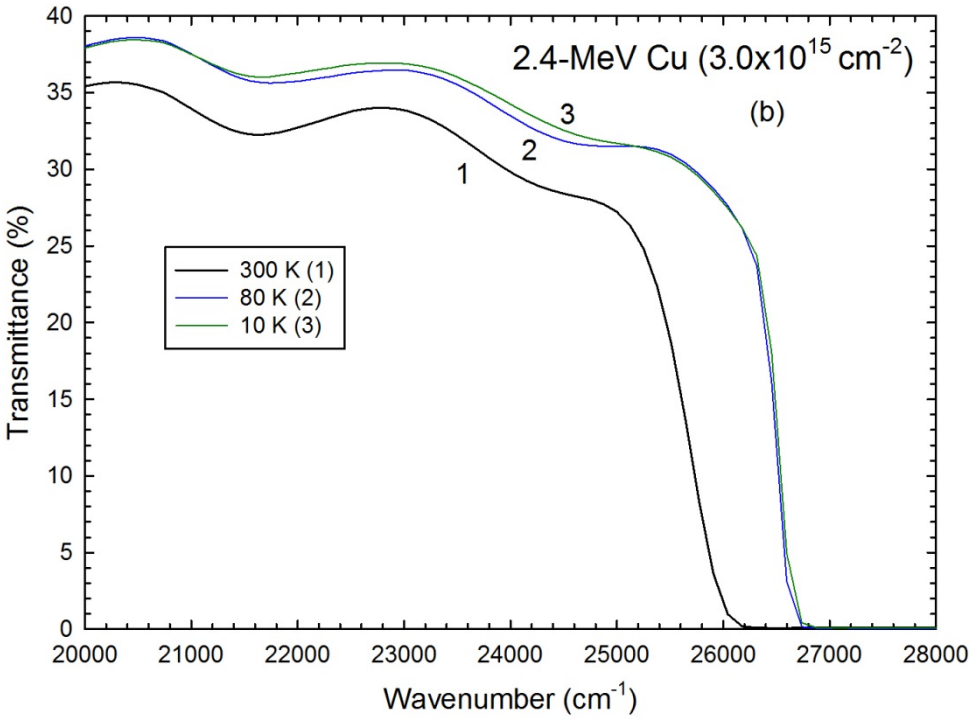
2.4-MeV Cu (3.0x10^15 cm^-2)
(b)
1
2
3
300 K (1)
80 K (2)
10 K (3)
Transmittance (%)
Wavenumber (cm^-1)
0
5
10
15
20
25
30
35
40
20000
21000
22000
23000
24000
25000
26000
27000
28000

Figure 5: Mean refractive index (n) of ceria films versus displacement per Ce atom (dpa) for the three electron energies. The dashed line marks the average n-value (2.46) for low dpa, and the solid line is a guide to the eyes.